

Discovery of an optical counterpart to the hyperluminous X-ray source in ESO 243-49

Roberto Soria^{1*}, George K. T. Hau², Alister W. Graham², Albert K. H. Kong³,
N. Paul M. Kuin¹, I-Hui Li², Ji-Feng Liu⁴ and Kinwah Wu¹

¹*Mullard Space Science Laboratory, University College London, Holmbury St Mary, Surrey RH5 6NT, UK*

²*Centre for Astrophysics and Supercomputing, Swinburne University of Technology, Hawthorn VIC 3122, Australia*

³*Institute of Astronomy and Department of Physics, National Tsing Hua University, Hsinchu 30013, Taiwan*

⁴*Harvard-Smithsonian Center for Astrophysics, 60 Garden st, Cambridge MA 02138, USA*

Accepted 2010 February 09

ABSTRACT

The existence of black holes of masses $\sim 10^2$ – $10^5 M_\odot$ has important implications for the formation and evolution of star clusters and supermassive black holes. One of the strongest candidates to date is the hyperluminous X-ray source HLX1, possibly located in the S0-a galaxy ESO 243-49, but the lack of an identifiable optical counterpart had hampered its interpretation. Using the *Magellan* telescope, we have discovered an unresolved optical source with $R = 23.80 \pm 0.25$ mag and $V = 24.5 \pm 0.3$ mag within HLX1's positional error circle. This implies an average X-ray/optical flux ratio ~ 500 . Taking the same distance as ESO 243-49, we obtain an intrinsic brightness $M_R = -11.0 \pm 0.3$ mag, comparable to that of a massive globular cluster. Alternatively, the optical source is consistent with a main-sequence M star in the Galactic halo (for example an M4.4 star at ≈ 2.5 kpc). We also examined the properties of ESO 243-49 by combining *Swift*/UVOT observations with stellar population modelling. We found that the overall emission is dominated by a ~ 5 Gyr old stellar population, but the UV emission at ≈ 2000 Å is mostly due to ongoing star-formation at a rate of $\sim 0.03 M_\odot \text{ yr}^{-1}$. The UV emission is more intense (at least a 9σ enhancement above the mean) North East of the nucleus, in the same quadrant as HLX1. With the combined optical and X-ray measurements, we put constraints on the nature of HLX1. We rule out a foreground star and a background AGN. Two alternative scenarios are still viable. HLX1 could be an accreting intermediate mass black hole in a star cluster, which may itself be the stripped nucleus of a dwarf galaxy that passed through ESO 243-49, an event which might have caused the current episode of star formation. Or, it could be a neutron star in the Galactic halo, accreting from an M4–M5 donor star.

Key words: galaxies: individual: ESO 243-49 – X-rays: binaries – ultraviolet: galaxies – black hole physics.

1 INTRODUCTION: ULTRALUMINOUS AND HYPERLUMINOUS X-RAY SOURCES

XMM-Newton and *Chandra* have discovered several non-nuclear X-ray sources in nearby galaxies, with luminosities up to two orders of magnitude higher than those observed from Galactic X-ray binaries. These are referred to as ultraluminous X-ray sources (ULXs; e.g., Grimm et al. 2003; Swartz et al. 2004; Roberts 2007). Those findings have challenged our current models of black hole (BH) formation and accretion. Isotropic, Eddington-limited luminosities $\gtrsim 10^{40} \text{ erg s}^{-1}$ would require BH masses $\gtrsim 100 M_\odot$, beyond the

upper limit for individual stellar collapses (Yungelson et al. 2008). Mildly super-Eddington luminosity (possibly due to large super-Eddington mass accretion) from particularly heavy stellar BHs ($M \sim 50 M_\odot$), associated with mildly anisotropic emission may explain X-ray luminosities up to $\sim \text{few} \times 10^{40} \text{ erg s}^{-1}$ without the need for more exotic astrophysical processes (Poutanen et al. 2007; Roberts 2007; King 2009).

Only a few non-nuclear sources have been observed at X-ray luminosities ≈ 0.7 – $1 \times 10^{41} \text{ erg s}^{-1}$. For example, in the Cartwheel (Wolter et al. 2006), in M 82 (Feng & Kaaret 2010), in NGC 2276 (Davis & Mushotzky 2004), and in NGC 5775 (Li et al. 2008). It is possible that such rare, extreme ULXs (sometimes known as hyperluminous X-ray

* E-mail: roberto.soria@mssl.ucl.ac.uk

sources, HLXs) may be powered by heavier BHs, formed through different channels: for example, in the collapsed core of a super star cluster, or within the nuclear star cluster of an accreted (and now disrupted) dwarf galaxy (King & Dehnen 2005; Bekki & Freeman 2003). Thus, HLXs may represent evidence of intermediate-mass BHs. However, the debate is far from settled, given the small number of HLXs known, and the possibility of confusion with background AGN. The strongest claim for an X-ray luminous intermediate-mass BH so far has been made for a recently discovered X-ray source (2XMM J011028.1–460421, hereafter HLX1: Farrell et al. 2009; Godet et al. 2009) apparently located in the galaxy ESO 243-49, or, at least, projected inside the $\mu_B = 25.0$ mag arcsec $^{-2}$ surface brightness isophote of that galaxy. Here, we report our discovery of the likely optical counterpart to this source, and our analysis of the UV emission in ESO 243-49. By determining the optical flux, and the X-ray/optical flux ratio, we test alternative models for the nature of this object. Our results strengthen the interpretation that the X-ray source belongs to ESO 243-49. We suggest that it is located inside a massive star cluster.

ESO 243-49 is an edge-on S0-a galaxy at a luminosity distance of 91 ± 6 Mpc ($z = 0.0224$, distance modulus 34.80 ± 0.15 : Caldwell & Rose 1997). The foreground extinction is very low, $A_V = 0.043$ mag (Schlegel et al. 1998). HLX1 appears projected $\approx 7''$ (≈ 3.1 kpc) to the North-East of ESO 243-49’s nucleus, and $\approx 1''.8$ (≈ 800 pc) above the galactic plane. HLX1 has been detected several times with *XMM-Newton*, *Chandra* and *Swift* between 2004 and 2009 (Farrell et al. 2009; Godet et al. 2009), with an unabsorbed luminosity in the 0.3–10 keV band varying between $\lesssim 5 \times 10^{40}$ erg s $^{-1}$ and $\approx 1 \times 10^{42}$ erg s $^{-1}$. We also examined a *ROSAT*/HRI observation of the field from 1996, when HLX1 was not detected to an upper limit of $\approx 5 \times 10^{40}$ erg s $^{-1}$. Its combination of extreme luminosity (if it really belongs to ESO 243-49), soft spectrum, and spectral changes on short timescales (Godet et al. 2009) makes it a unique object among the ULX/HLX class. Its apparent location in an S0 galaxy is also puzzling, because such galaxies are usually dominated by an old stellar population. For example, the integrated brightnesses of ESO 243-49 are (Cousins) $B = 14.92 \pm 0.09$ mag, (Cousins) $R = 13.48 \pm 0.09$ mag and (2MASS) $K = 10.70 \pm 0.05$ mag (from NED¹), which are indicative of a characteristic stellar age \sim a few Gyr (Section 4). Such moderately old populations were not previously known to host luminous ULXs or HLXs. For these reasons, it was speculated that the source might be a background AGN or a foreground neutron star, even though its X-ray properties are also very unusual for both classes of objects (Section 5).

2 X-RAY POSITION OF HLX1

We used the *Chandra* High Resolution Camera (HRC-I) dataset from 2009 August 17 (available in the public archives; processed with ASCDVER=8.0) to determine the position of the X-ray source HLX1. We checked that there

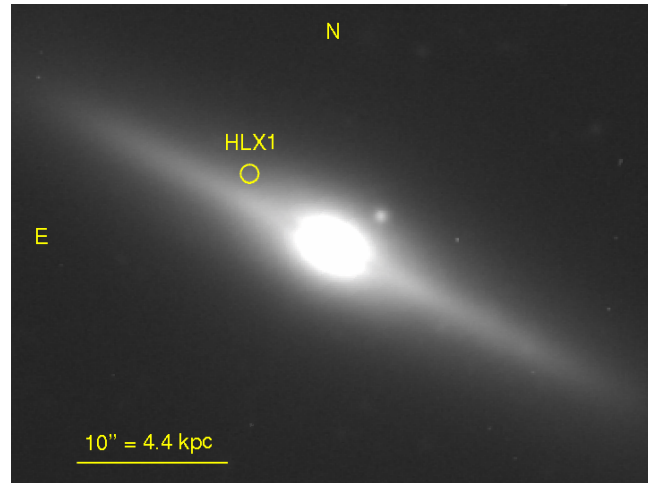


Figure 1. *Magellan*/IMACS *R*-band image of ESO 243-49, with the X-ray position of HLX1 marked by a circle of $0''.5$ radius (combined astrometric uncertainty of the X-ray and optical images).

Telescope	Date	Band	Exposure	
<i>Magellan</i> Baade	2009 Aug 26	R	540 s	
		V	540 s	
<i>Swift</i> /UVOT	2008 Oct 24	<i>u</i>	380 s	
		<i>uvw1</i>	760 s	
		<i>uvw2</i>	196 s	
	2008 Oct 25	<i>uvw2</i>	1264 s	
		2008 Nov 01	<i>u</i>	730 s
	<i>uvw1</i>		1690 s	
	<i>uvw2</i>		2639 s	
	2008 Nov 07	<i>u</i>	1210 s	
		<i>uvw1</i>	2410 s	
		<i>uvw2</i>	3278 s	
	2008 Nov 08	<i>uvw2</i>	582 s	
		2008 Nov 14	<i>u</i>	980 s
	<i>uvw1</i>		1960 s	
	<i>uvw2</i>		3814 s	
	2009 Aug 05	<i>uvw2</i>	9753 s	
		2009 Aug 06	<i>uvw2</i>	9132 s
			2009 Aug 16	<i>uvw2</i>
		<i>uvw2</i>		681 s
		2009 Aug 18	<i>uvw2</i>	6032 s
			2009 Aug 19	<i>uvw2</i>
		2009 Aug 20		<i>uvw2</i>
			2009 Nov 02	<i>uvw2</i>
		2009 Nov 14		<i>uvw2</i>
			2009 Nov 20	<i>uvw2</i>
		2009 Nov 21		<i>uvw2</i>
			2009 Nov 28	<i>uvw2</i>
		2009 Nov 29		<i>uvw2</i>
2009 Dec 05			<i>uvw2</i>	2993 s
		2009 Dec 19	<i>uvw2</i>	2518 s
2009 Dec 26			<i>uvw2</i>	2774 s
		2010 Jan 02	<i>uvw2</i>	2590 s
2010 Jan 08	<i>uvw2</i>		4348 s	
	2010 Jan 13	<i>uvw2</i>	3577 s	
2010 Jan 15		<i>uvw2</i>	3068 s	
	2010 Jan 22	<i>uvw2</i>	2945 s	

Table 1. Optical/UV observation log.

¹ <http://nedwww.ipac.caltech.edu>

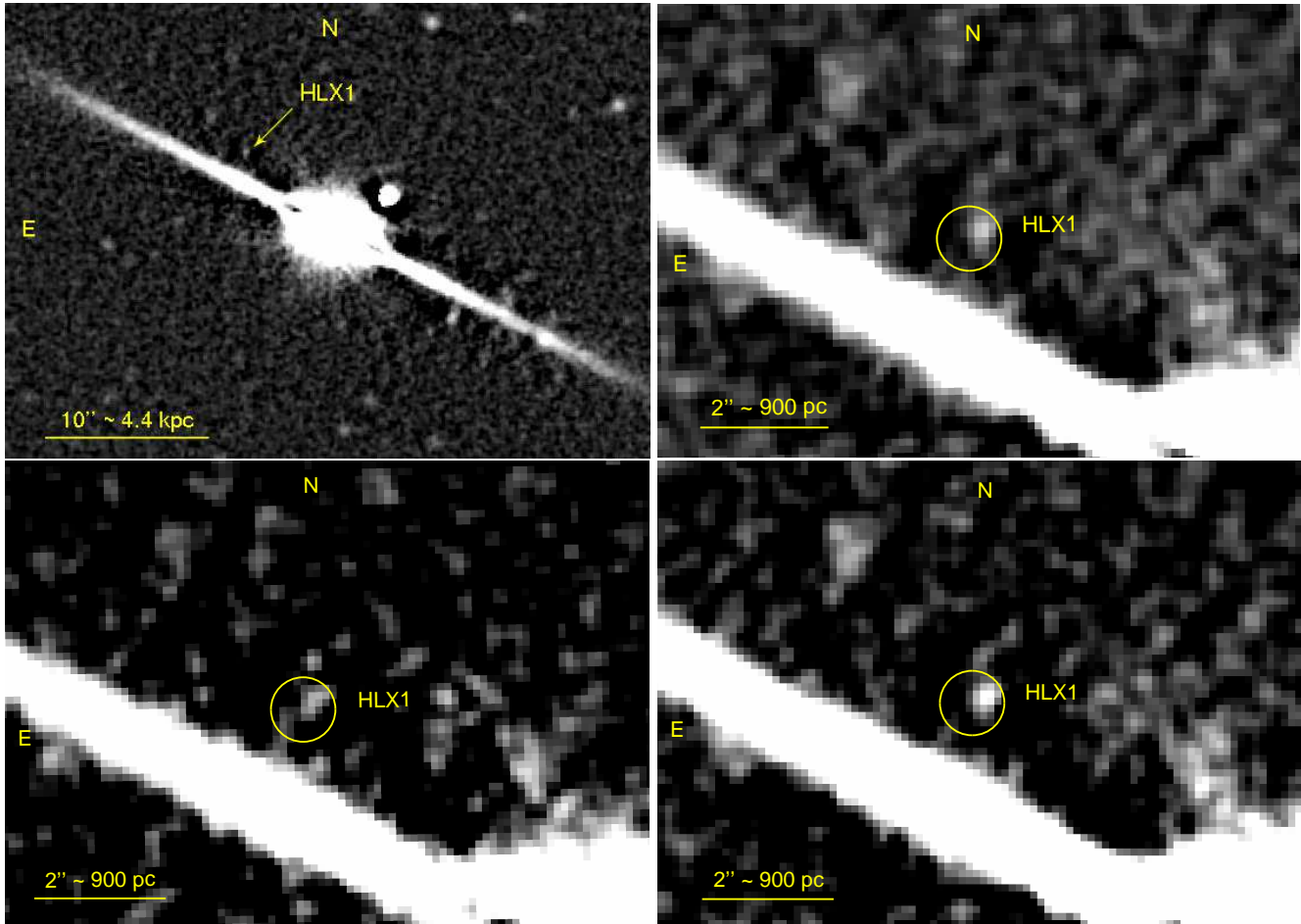


Figure 2. *Top left:* differential R -band image of ESO 243-49, with a median-filter smoothed image subtracted from the original image (logarithmic greyscale). The source marked with an arrow has a 4σ significance and is located near the X-ray position of HLX1. *Top right:* zoomed-in view of the field around HLX1, in the R -band residual image (square-root greyscale). The *Chandra*/HRC-I position of HLX1 is marked by a circle of $0''.5$ radius (combined astrometric uncertainty of the X-ray and optical images). Both the top and bottom panel images have been Gaussian-smoothed with a kernel radius of 2 pixels ($0''.22$), for display purposes only. *Bottom left:* Gaussian-smoothed field around HLX1, in the V -band residual image (logarithmic greyscale); an optical counterpart is located at the same position with a 3σ significance. *Bottom right:* Gaussian-smoothed field around HLX1, from the combined R -band plus V -band residual images.

are no processing offsets associated with that dataset. Applying any standard source-finding routines (e.g., *celldetect* or *wavdetect* in CIAO 4.0, or *imexamine* in IRAF) we find that HLX1 is a well-isolated, on-axis, point-like X-ray source with ≈ 900 net counts; it is located at RA = $01^h 10^m 28^s .27$, Dec = $-46^\circ 04' 22''.3$, with an error radius for the centroid position $\approx 0''.03$. We obtain exactly the same centroid position when we examine the unbinned HRC-I image ($0''.125/\text{pixel}$), or when we bin by 2, or by 4. The 90% uncertainty circle of the HRC-I absolute position has a radius of $0''.4^2$. We assessed whether the absolute astrometry of the *Chandra*/HRC-I image could be improved by using optical/IR/radio counterparts with well-known positions. There are only two other (fainter) X-ray sources with > 25 counts located within $\approx 5'$ of the aimpoint; neither has a known counterpart. A few other X-ray sources are located farther from the aim point, and therefore have a very elongated PSF and are not good choices for astrometry calibration.

We also tried registering the three *Chandra* sources nearest to the aimpoint onto the corresponding *XMM-Newton* sources, and then some of the other *XMM-Newton* sources onto their optical/IR counterparts, but we concluded that this does not improve either the precision or the accuracy of the original *Chandra* astrometry.

3 OPTICAL COUNTERPART OF HLX1

We observed the source on 2009 August 26 with the IMACS Long Camera (SITE CCD) on the 6.5-m Baade *Magellan* telescope. We took a series of 3×180 s exposures in each of the Bessell B, V, R filters (Bessell 1979). However, the B images are badly affected by a non-optimal focus and cannot be used for this work. The seeing was $\approx 0''.7$, and the airmass was ≈ 1.2 . We used the STARLINK program *gaia*, as well as standard IRAF packages, to analyze the optical images. We calibrated the astrometry of the *Magellan* images by using stellar positions from the Guide Star Catalog Version 2.3

² <http://cxc.harvard.edu/cal/ASPECT/celmon/>

UVOT Filter	Brightness (mag)	λ_{eff} (Å)	ν_{eff} (10^{15} Hz)	Flux Density (10^{-16} erg s $^{-1}$ cm $^{-2}$ Å $^{-1}$)	Flux Density (10^{-26} erg s $^{-1}$ cm $^{-2}$ Hz $^{-1}$)
<i>uvw2</i>	18.06 ± 0.12	2030	1.477	3.1 ± 0.3	0.045 ± 0.005
<i>uvw1</i>	17.07 ± 0.12	2634	1.138	6.3 ± 0.6	0.154 ± 0.015
<i>u</i>	15.7 ± 0.2	3501	0.856	16.6 ± 2.4	0.85 ± 0.12

Table 2. Integrated brightness of ESO 243-49 in the UVOT bands (3σ confidence level).

(Lasker et al. 2008). Our optical astrometry is accurate to $\approx 0''.3$.

At first inspection, any faint optical counterpart to the X-ray source would be swamped by the strong stellar light from the main galaxy (Figure 1). However, at closer inspection we noted that there is an excess of counts, consistent with a point source, in the *R*-band image at the position of HLX1. To visualize this source, we generated a smoothed image with a 17×17 pixel median filtering. We then subtracted the smoothed image from the original image. This brings up residuals consistent with point-like sources, including a source in the X-ray error circle of HLX1 (Figure 2, top panels). The optical source is located at RA = $01^h 10^m 28^s.25$, Dec = $-46^\circ 04' 22''.2$, which is $\lesssim 0''.3$ from the central X-ray position, and within the combined optical and X-ray positional uncertainties ($\approx 0''.5$). There are no other optical sources of comparable or higher brightness within a few arcsec, outside the galactic plane. As a further check that the optical source is not for example a cosmic ray, we analysed each of the three 180-s sub-exposures separately, and found it in each of them. To quantify the significance of this detection, we measured the counts in a 5×5 pixel box centred on the source in the residual image (multiplied by an aperture correction factor of 1.1, to account for the small fraction of source counts falling outside the box). We compared those counts with the mean and the distribution of counts in 20 5×5 pixel boxes covering the background sky around HLX1 (above and below the disk plane of the galaxy). We obtain that the source detection is significant to 4σ . Moreover, here we are not looking for any 4σ source randomly positioned around the galaxy: we are specifically investigating whether there is a source within $\approx 0''.5$ of the X-ray position. Based on the source significance combined with the positional coincidence, we conclude that this optical source is real and is the most likely candidate for the optical counterpart of HLX1. We then repeated the same analysis for the *V*-band image, and found a source at 3σ significance in the residual image, at the same position as the source in the *R*-band image (Figure 2, bottom left panel). The positional coincidence further strengthens our identification as the likely optical counterpart of HLX1. Finally, we combined the *R* and *V* residual images, which further improves the signal-to-noise ratio (Figure 2, bottom right).

We performed an aperture photometry measurement of this source, and used isolated point-like objects in the field to calculate the aperture correction. To convert from count rates to fluxes, at first we tried using stars with photometric measurements in the Naval Observatory Merged Astrometric Dataset (NOMAD) Catalog (Monet et al. 2003; Zacharias et al. 2005). However, we did not find stars with sufficiently reliable and accurate brightnesses within the field of view of the *Magellan* image. We then downloaded a

series of *V* and *R* exposures taken with the Wide Field Imager (WFI) on the 2.2-m MPG/ESO telescope at La Silla³, which obviously cover a much larger field of view around ESO 243-49. We measured the brightness of a few galaxies with reliable NED values to calibrate the photometry of the WFI field, and applied it to sources that are also included in the *Magellan* images. From that, we bootstrapped the conversion between count rate and magnitudes in the *Magellan* images. For ESO 243-49, we obtain an integrated (Cousin) brightness $R = 13.5 \pm 0.1$ mag, $V = 14.2 \pm 0.1$. This is in agreement with the values listed in NED, and with the expected colour of a moderately old population; it shows that our method is reliable⁴. Using the same photometric calibration and accounting for the aperture correction of a point-like source, we determined the brightness of the optical counterpart to HLX1. We obtain a brightness $R = 23.80 \pm 0.25$ mag, $V = 24.5 \pm 0.3$ mag. If the object is located in ESO 243-49, its intrinsic brightness (corrected for Galactic extinction and taking into account the distance uncertainty) is $M_R = -11.0 \pm 0.3$ mag, $M_V = -10.4 \pm 0.3$ mag.

4 UV EMISSION FROM ESO 243-49

In the UV bands, ESO 243-49 was observed several times between 2008 October 24 and 2010 January 22, with the 30-cm UV/Optical Telescope (UVOT) on board *Swift*. The total exposure times were 3.3 ks in the *u* band, 6.7 ks in *uvw1*, 4.9 ks in *uvw2*, and 94.1 ks in *uwv2*. In fact, the *uvw2* exposure proved to be too short for meaningful analysis, and we do not use it further. See Table 1 for a log of our observations. We retrieved the *Swift*/UVOT datasets (all observations through the end of 2009 November) from the HEASARC archive, and processed them using standard FTOOLS tasks. We applied the mod8 and aspect corrections to each of the individual images, which were taken at various space craft roll angles, and with slightly different offsets. Most images were provided with a $1''$ pixel size. We summed them using the *uvotimsum* task, and resampled them to a $0''.5$ pixel size. We checked the astrometry by correlating UVOT sources with those detected in the *Magellan* images, as well as source positions from the USNO-B1.0 Catalog (Monet et al. 2003). In particular, we determined the position error between 23 sources common to the *R*-band and the

³ The WFI images were taken as part of a programme by H. Boehringer, to look for high-redshift clusters.

⁴ As a further check, we also examined the count rate to magnitude conversion factors from the *Magellan* exposure time calculator, and found that they agree with our conversion factors, within ≈ 0.3 mag.

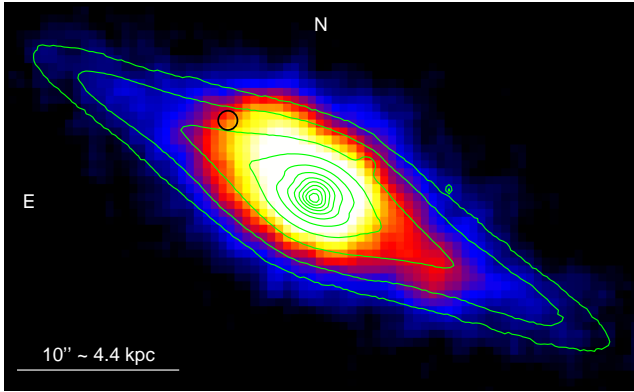


Figure 3. *Swift*/UVOT false-colour image of ESO 243-49 in the *uvw2* band, with *R*-band surface brightness contours overlaid (square root scale). The X-ray position of HLX1 is marked with a black circle (error radius $0''.6$: combined astrometric uncertainty of the X-ray and UV images). While the *R*-band contours are highly symmetric, the *uvw2* emission extends more strongly to the North East of the nucleus, with a $> 9\sigma$ significance of the excess. The flux density scale corresponding to the *uvw2* false-colours is as such: blue between $\approx 0.2\text{--}0.7 \times 10^{-18} \text{ erg s}^{-1} \text{ cm}^{-2} \text{ \AA}^{-1} \text{ arcsec}^{-2}$ (*uvw2* $\approx 26\text{--}24.7 \text{ mag arcsec}^{-2}$); red between $\approx 0.7\text{--}1.4 \times 10^{-18} \text{ erg s}^{-1} \text{ cm}^{-2} \text{ \AA}^{-1} \text{ arcsec}^{-2}$ (*uvw2* $\approx 24.7\text{--}23.9 \text{ mag arcsec}^{-2}$); yellow between $\approx 1.4\text{--}2.1 \times 10^{-18} \text{ erg s}^{-1} \text{ cm}^{-2} \text{ \AA}^{-1} \text{ arcsec}^{-2}$ (*uvw2* $\approx 23.9\text{--}23.5 \text{ mag arcsec}^{-2}$); white $\gtrsim 2.1 \times 10^{-18} \text{ erg s}^{-1} \text{ cm}^{-2} \text{ \AA}^{-1} \text{ arcsec}^{-2}$ (*uvw2* $\lesssim 23.5 \text{ mag arcsec}^{-2}$).

combined *uvw2* image, and found that the positions are consistent with a root-mean-square spread of $0''.18$, with a 95% confidence level of $\approx 0''.4$. We conservatively took a combined error circle of radius $0''.6$ when comparing UVOT and *Chandra* positions. The observed full-width half-maximum of point-like sources in the combined images goes from $\approx 3''.0$ for the *u* filter image to $\approx 3''.6$ for the *uvw2* filter image, which is a stack of 90 sub-exposures; the observed full-width half-maximum in each *uvw2* subexposure is $\approx 3''.4$. We performed aperture photometry with *uvotsource* to derive initial count rates. Filter transmission curves and conversion factors between UVOT count rates and fluxes or magnitudes are detailed in Poole et al. (2008). However, those factors were derived for an aperture of $5''$ on point sources. In our case, we are also interested in the total emission from extended regions. Therefore, we calculated appropriate aperture corrections for extended emission, using the extended UVOT point-spread-function (Breeveld et al. 2010), and the appropriate HEASARC *Swift*/UVOT CALDB files.

We do not detect a point-like UV counterpart at the X-ray position, to an upper limit *uvw2* $\approx 22.7 \text{ mag}$; this corresponds to a flux $f_\nu \approx 5.9 \times 10^{-7} \text{ Jy} = 5.9 \times 10^{-30} \text{ erg s}^{-1} \text{ cm}^{-2} \text{ Hz}^{-1}$ at an effective frequency of $1.477 \times 10^{15} \text{ Hz}$, or $\approx 2030 \text{ \AA}$ (Poole et al. 2008). The non-detection of a point-like counterpart is not surprising, given the full-width half-maximum of the point spread function. However, the UVOT data provide interesting information on the host galaxy environment. For the whole galaxy, we measure a total brightness (uncorrected for extinction) $u = 15.7 \pm 0.2 \text{ mag}^5$, *uvw1* $= 17.07 \pm 0.12 \text{ mag}$, *uvw2* $= 18.06 \pm 0.12 \text{ mag}$

(3σ uncertainties). The *uvw2* brightness corresponds to a flux $f_\nu \approx 4.5 \times 10^{-5} \text{ Jy} = 4.5 \times 10^{-28} \text{ erg s}^{-1} \text{ cm}^{-2} \text{ Hz}^{-1}$ at $\nu = 1.477 \times 10^{15} \text{ Hz}$ (Table 2).

First, we tested whether these UV brightnesses and colours are consistent with the moderately old population suggested by the optical colours and morphology of ESO 243-49. We downloaded⁶ an optical spectrum of the galaxy from the 6dF Galaxy Survey Database (Jonker et al. 2004; Jones et al. 2009). From the observed strength of the $H\beta$ absorption line, and of the Fe5270 and Fe5335 indices (Worthey 1994; Worthey et al. 1994), we estimate that the dominant population has an age $\approx 4.5_{-2.5}^{+4.0}$ Gyr (assuming solar metallicity). As a further check of this observational estimate, we ran instantaneous star-formation simulations with Starburst99 (Leitherer et al. 1999; Vazquez & Leitherer 2005), to determine the expected brightness and colours of stellar populations with ages ~ 2 to 8 Gyr. In particular, we find that a population with a single age of 4.5 Gyr, initial stellar mass $= 6 \times 10^{10} M_\odot$ and solar metallicity is predicted to have $R \approx 13.5 \text{ mag}$, $B \approx 15.0 \text{ mag}$, $U \approx 15.5 \text{ mag}$, *uvw1* $\approx 17.3 \text{ mag}$, *uvw2* $\approx 20 \text{ mag}$ (at the distance of ESO 243-49 and after adding the foreground extinction $A_V = 0.043 \text{ mag}$). Such values are indeed similar to the observed colours, except for *uvw2*. More detailed population modelling of the galaxy is beyond the scope of this work: here, we simply want to stress that the emission in all bands up to *uvw1* (effective wavelength 2634 \AA) is dominated by a moderately old stellar population, but extra UV emission from a much younger population dominates the *uvw2* band. Adding a population with ongoing star-formation rate $\approx 0.03 M_\odot \text{ yr}^{-1}$ is sufficient to explain the bright far-UV emission, while it contributes little to the other bands, compared to the emission from the older population (Table 3).

We then examined the emission from the young stellar population, which dominates the *uvw2* image (Figure 3). The emission appears asymmetric, and does not match the *R*-band surface brightness contours well. In particular, it is clear already from an eye-ball inspection that the *uvw2* emission extends more strongly to the North East of the nucleus (the same quadrant as HLX1). In order to quantify the degree of asymmetry, we used the highly symmetric *R*-band isophotes to define four quadrants (bounded by the galactic plane and the normal to the plane), and extracted the *uvw2* flux in each of them. Based on our best optical/UV alignment, we find that the flux in the North East quadrant is $\approx 40\%$ higher than the average flux of the other three quadrants; that corresponds to a 13σ enhancement. Excluding a $4''$ -box around the nucleus, we measured the following *uvw2* net count rates in the four quadrants. North-East: $0.1100 \pm 0.0017 \text{ counts s}^{-1}$; North-West: $0.0784 \pm 0.0016 \text{ counts s}^{-1}$; South-West: $0.0792 \pm 0.0016 \text{ counts s}^{-1}$; South-East: $0.0794 \pm 0.0016 \text{ counts s}^{-1}$. We tried different definitions for the size of the four quadrants, including/excluding the nucleus. We repeated the exercise after shifting the placement of the four quadrants by $\pm 0''.4$, to account for the relative astrometric uncertainty between the UVOT and Magellan images and the small uncertainty in the position angle of the major axis. We obtain that the emission en-

⁵ The difference between the UVOT *u* brightness and the standard Johnson U is $\lesssim 0.05 \text{ mag}$ (Poole et al. 2008).

⁶ From <http://www-wfau.roe.ac.uk/6dFGS>

Band	Obs. Brightness (mag)	Obs. Flux Density (10^{-16} CGS)	Model Flux Density Old Population (10^{-16} CGS)	Model Flux Density Young Population (10^{-16} CGS)	Model Brightness Old Population (mag)	Model Brightness Combined (mag)
<i>uvw2</i>	18.06 ± 0.12	3.1 ± 0.3	≈ 0.5	≈ 2.5	≈ 20	≈ 18.1
<i>uvw1</i>	17.07 ± 0.12	6.3 ± 0.6	≈ 5	≈ 1.1	≈ 17.3	≈ 17.1
<i>u</i>	15.7 ± 0.2	16.6 ± 2.4	≈ 19	≈ 0.6	≈ 15.5	≈ 15.5

Table 3. Observed brightness of ESO 243-49 in the UVOT bands, compared with the predicted brightness of a 4.5-Gyr-old population (initial stellar mass = $6 \times 10^{10} M_{\odot}$, solar metallicity, foreground extinction $A_V = 0.043$ mag) with an additional contribution from ongoing star formation at a rate $\approx 0.03 M_{\odot} \text{ yr}^{-1}$. Flux units are $10^{-16} \text{ erg s}^{-1} \text{ cm}^{-2} \text{ \AA}^{-1}$. We used Starburst99 (Leitherer et al. 1999; Vazquez & Leitherer 2005) for the model simulations.

hancement in the North East quadrant is always significant to $\gtrsim 9\sigma$. The excess *uvw2* emission in that part of the galaxy may be interpreted as a more recent or intense phase of star formation. We find no statistically-significant enhancements or asymmetries in the *uvw1* and *u* bands, in agreement with our estimate that the emission in those bands is dominated by the old stellar population. We can plausibly say that the young/starforming component is not as symmetrically distributed as the old population.

5 DISCUSSION

If the X-ray source HLX1 is proven to be an accreting BH with mass $\sim 10^3$ – $10^4 M_{\odot}$, there would be important implications on models of galaxy formation and evolution. Identifying its optical counterpart gives a crucial constraint on its nature. We have found an unresolved optical source within its X-ray error circle, and it is likely to be physically associated to HLX1. Assuming a direct association, we calculate an X-ray/optical flux ratio, using the standard definition (Hornschemeier et al. 2001): $\log(f_X/f_R) = \log f_X + 5.5 + R/2.5$, where f_X is the intrinsic flux in the 0.3–10 keV band (taken from Godet et al. 2009, and our spectral analysis of the *Swift*/XRT data). We obtain $f_X/f_R \approx 800$ – 1000 for the X-ray high state of 2009 August, and $f_X/f_R \approx 500$ for the “average” X-ray state where the source was more often observed over 2008–2009; such ratio is only slightly dependent on the choice of X-ray spectral model. The observed X-ray/optical flux ratio is much higher than expected for AGN, which have typical $f_X/f_R \lesssim 10$ (Laird et al. 2009; Bauer et al. 2004). A number of distant, faint AGN are undetected in the optical band because of extinction, which is not an issue for this object (Farrell et al. 2009; Godet et al. 2009). In particular, AGN with a 0.5–2 keV flux of $\approx 5 \times 10^{-13} \text{ erg s}^{-1} \text{ cm}^{-2}$ are rare ($N \approx 0.5 \text{ deg}^{-2}$; Hasinger 1998) and have always been easily identified in other bands. Moreover, the red colour of the optical counterpart ($V - R = 0.7 \pm 0.4$) suggests that the optical emission is not dominated by the Rayleigh-Jeans tail of an accretion disk spectrum.

Neutron stars are a class of objects that can reach X-ray/optical flux ratios $\gtrsim 1000$, with thermal X-ray emission from their surface. We note (Soria et al., in prep.) that the X-ray spectra of HLX1 can also be fitted with a neutron star atmosphere model (e.g., *nsa* in XSPEC) plus power-law. Such models suggest a characteristic distance ≈ 1.5 – 2.5 kpc, placing the source in the Galactic halo. The corresponding

0.3–10 keV luminosity would be \approx a few $\times 10^{32} \text{ erg s}^{-1}$. Intriguingly, this is a range of luminosities where quiescent low-mass X-ray binaries also show a thermal plus power-law spectrum, with the relative contribution of the power-law decreasing as the source gets brighter (Jonker et al. 2004). In this scenario, the apparent optical brightness $R \approx 23.8$ mag implies $M_R \approx 11.8$ – 12.8 mag, consistent with a main-sequence M4.4–M5.2 donor star, with an initial mass ≈ 0.13 – $0.17 M_{\odot}$ (Knigge 2006; Girardi et al. 2000). A late-type M star is also consistent with the observed red colour. Thus, we cannot rule out the possibility of an accreting neutron star in the Galactic halo, from the optical data. In this case, the excess UV emission North East of the nucleus in ESO 243-49 is purely coincidental.

The optical counterpart of HLX1 does not stick out like a unique object in the field. In the *R*-band residual image, we identified a few other sources consistent with globular clusters around ESO 243-49, with comparable brightnesses (Figure 2, top panel). If the HLX1 counterpart is also a globular cluster in that galaxy, its optical luminosity would place it between the Milky Way globular cluster ω Cen ($M_V = -10.3$ mag, $M_R = -10.8$ mag, $M_{\text{tot}} \approx 2.8 \times 10^6 M_{\odot}$: Harris 1996; van der Marel & Anderson 2010) and the Andromeda cluster G1 ($M_V = -11.2$ mag, $M_R = -11.8$ mag, $M_{\text{tot}} \approx 5 \times 10^6 M_{\odot}$: Graham & Spitler 2009), which is a strong candidate for the presence of an $\approx 2 \times 10^4 M_{\odot}$ BH (Gebhardt et al. 2005, but see Baumgardt et al. 2003).

There are a number of scenarios for the formation of an intermediate-mass BH inside a massive star cluster. In a young star cluster, runaway core collapse and coalescence of the most massive stars can occur over a timescale $\lesssim 3$ Myrs and can result in the formation of a supermassive star, which can quickly collapse into a BH (Portegies Zwart & McMillan 2002; Freitag et al. 2006). In an old globular cluster, an intermediate-mass BH can be formed from the merger of stellar-mass BHs and neutron stars over a timescale $\sim 10^9$ yr (O’Leary et al. 2006). Subsequent capture and disruption of a cluster star may then provide the accretion rate required to explain the X-ray luminosity. In this scenario, HLX1 and its host star cluster are unrelated to the ongoing star formation in the bulge of ESO 243-49.

The most intriguing scenario is that some massive star clusters may have been the nuclear clusters of satellite galaxies accreted and tidally disrupted by a more massive galaxy. Dwarf galaxies are the most common type of galaxies in clusters (e.g., Binggeli et al. 1985) and many of them are nucleated (e.g., Graham & Guzman 2003; Côté et al. 2006). In many cases, a nuclear cluster may coexist with a nuclear

BH (Graham & Spitler 2009; Seth et al. 2008). This may end up in the halo of a bigger galaxy after a merger. ω Cen itself may have originated from the nuclear star cluster of an accreted dwarf (Bekki & Freeman 2003). Similar suggestions have been made for a group of clusters in NGC 5128 (Peng et al. 2002; Chattopadhyay et al. 2009). The recent or ongoing star formation in ESO 243-49 may have been triggered by the passage and tidal disruption of the satellite galaxy, perhaps along the South-West to North-East direction, since *uvw2* emission is stronger on that side (Section 4). During its passage through ESO 243-49, the compact nucleus of the satellite dwarf may also have collected gas from the main galaxy (Pflamm-Altenburg & Kroupa 2009), and this may perhaps be fuelling a nuclear BH. In this scenario, HLX1 may be the intermediate-mass BH located in the nuclear cluster of that accreted satellite.

In summary, we have identified a point-like optical counterpart for HLX1 in ESO 243-49 in the *Magellan* images. The optical brightness and colour are consistent with a massive star cluster in ESO 243-49, or with a main-sequence M4–M5 star in the Milky Way halo, at ≈ 1.5 –2.5 kpc. The galaxy is dominated by a ~ 5 Gyr old population, but shows excess emission in the *Swift*/*UVOT* *uvw2* band, consistent with a recent episode of star formation. The far-UV emission has an asymmetric shape and is stronger to the North East of the nucleus, roughly in the direction of HLX1.

ACKNOWLEDGMENTS

We thank Mark Cropper, Rosanne di Stefano, Sean Farrell, Jeanette Gladstone, Craig Heinke, Erik Hooverstein, Pavel Kroupa, Tom Maccarone, Greg Sivakoff, Lee Spitler and Doug Swartz for discussions. We thank the referee for a detailed review and comments. RS acknowledges hospitality and financial assistance at Tsing Hua University (Taiwan), and hospitality at the University of Sydney, during part of this work.

REFERENCES

- Bauer, F. E., Alexander, D. M., Brandt, W. N., Schneider, D. P., Treister, E., Hornschemeier, A. E., & Garmire, G. P. 2004, *AJ*, 128, 2048
- Baumgardt, H., Makino, J., Hut, P., McMillan, S., & Portegies Zwart, S. 2003, *ApJ*, 589, L25
- Bessell, M. S. 1979, *PASP*, 91, 589
- Bekki, K., & Freeman, K. C. 2003, *MNRAS*, 346, L11
- Binggeli, B., Sandage, A., & Tammann, G. A. 1985, *AJ*, 90, 1681
- Breeveld, A.A., et al. 2010, *MNRAS*, submitted
- Caldwell, N., & Rose, J. A. 1997, *AJ*, 113, 492
- Chattopadhyay, A. K., Chattopadhyay, T., Davoust, E., Mondal, S., & Sharina, M. 2009, *ApJ*, 705, 1533
- Côté, P., et al. 2006, *ApJS*, 165, 57
- Davis, D. S., & Mushotzky, R. F. 2004, *ApJ*, 604, 653
- Farrell, S. A., Webb, N. A., Barret, D., Godet, O., & Rodrigues, J. M. 2009, *Nature*, 460, 73
- Feng, H., & Kaaret, P. 2010, *ApJ*, submitted
- Freitag, M., Gürkan, M. A., & Rasio, F. A. 2006, *MNRAS*, 368, 141
- Gebhardt, K., Rich, R. M., & Ho, L. C. 2005, *ApJ*, 634, 1093
- Girardi, L., Bressan, A., Bertelli, G., & Chiosi, C. 2000, *A&AS*, 141, 371
- Godet, O., Barret, D., Webb, N. A., Farrell, S. A., & Gehrels, N. 2009, *ApJ*, 705, L109
- Graham, A. W., & Guzmán, R. 2003, *AJ*, 125, 2936
- Graham, A. W., & Spitler, L. R. 2009, *MNRAS*, 397, 2148
- Grimm, H.-J., Gilfanov, M., & Sunyaev, R. 2003, *MNRAS*, 339, 793
- Harris, W. E. 1996, *AJ*, 112, 1487
- Hasinger, G. 1998, *AN*, 319, 37
- Hornschemeier, A. E., et al. 2001, *ApJ*, 554, 742
- Jones, D. H., et al. 2004, *MNRAS*, 355, 747
- Jones, D. H., et al. 2009, *MNRAS*, 399, 683
- Jonker, P. G., Galloway, D. K., McClintock, J. E., Buxton, M., Garcia, M., & Murray, S. 2004, *MNRAS*, 354, 666
- King, A. R. 2009, *MNRAS*, 393, L41
- King, A. R., & Dehnen, W. 2005, *MNRAS*, 357, 275
- Knigge, C. 2006, *MNRAS*, 373, 484
- Laird, E. S., et al. 2009, *ApJS*, 180, 102
- Lasker, B. M., et al. 2008, *AJ*, 136, 735
- Leitherer, C., et al. 1999, *ApJS*, 123, 3
- Li, J.-T., Li, Z., Wang, Q. D., Irwin, J. A., & Rossa, J. 2008, *MNRAS*, 390, 59
- Monet, D. G., et al. 2003, *AJ*, 125, 984
- O’Leary, R. M., Rasio, F. A., Fregeau, J. M., Ivanova, N., & O’Shaughnessy, R. 2006, *ApJ*, 637, 937
- Peng, E. W., Ford, H. C., Freeman, K. C., & White, R. L. 2002, *AJ*, 124, 3144
- Pflamm-Altenburg, J., & Kroupa, P. 2009, *MNRAS*, 397, 488
- Poole, T.S., et al. 2008, *MNRAS*, 383, 627
- Portegies Zwart, S. F., & McMillan, S. L. W. 2002, *ApJ*, 576, 899
- Poutanen, J., Lipunova, G., Fabrika, S., Butkevich, A. G., & Abolmasov, P. 2007, *MNRAS*, 377, 1187
- Roberts, T. P. 2007, *Ap&SS*, 311, 203
- Schlegel, D. J., Finkbeiner, D. P., & Davis, M. 1998, *ApJ*, 500, 525
- Seth, A., Agüeros, M., Lee, D., & Basu-Zych, A. 2008, 678, 116
- Swartz, D. A., Ghosh, K. K., Tennant, A. F., & Wu, K. 2004, *ApJS*, 154, 519
- van der Marel, R. P., & Anderson, J. 2010, *ApJ*, 710, 1063
- Vazquez, G. A., & Leitherer, C. 2005, *ApJ*, 621, 695
- Wolter, A., Trinchieri, G., & Colpi, M. 2007, *MNRAS*, 373, 1627
- Worthey, G. 1994, *ApJS*, 95, 107
- Worthey, G., Faber, S. M., Gonzalez, J. J., & Burstein, D. 1994, *ApJS*, 94, 687
- Yungelson, L. R., van den Heuvel, E. P. J., Vink, J. S., Portegies Zwart, S. F., & de Koter, A. 2008, *A&A*, 477, 223
- Zacharias N., Monet D. G., Levine S. E., Urban S. E., Gaume R., & Wycoff G. L. 2005, *Vizier on-line NOMAD Catalog*